PHYSICAL REVIEW A VOLUME 25, NUMBER 3 MARCH 1982

Properties of high-lying doubly excited states of H^-

C. D. Lin
Department of Physics, Kansas State University, Manhattan, Kansas 66506
(Received 7 October 1981)

Doubly excited states of H^- lying below the hydrogenic $N=3$ and 4 thresholds are investigated in hyperspherical coordinates. Adiabatic potential curves are calculated using the recently developed analytical channel functions and approximate resonance energies, and their classifications are described. It is found that the present classification differs from the recent work by Gailitis for $^3P^o$ and $^1D^e$ states. Angular correlations for doubly excited states below $H(N=2)$ and $H(N=3)$ thresholds are also investigated for $^{1,3}S^o$, $^{1,3}P^o$, and $^{1,3}D^e$ symmetries. States belonging to different channels are found to have a high degree of different angular correlations.

I. INTRODUCTION

Doubly excited states of H^- lying below the $N=2$ threshold of H have been the subject of considerable theoretical and experimental investigations in the 60's and early 70's. Many elaborate theoretical calculations based upon close-coupling approximations,[1] Feshbach projection techniques,[2] and complex coordinate rotations[3] have been used to calculate the positions and widths of these multichannel resonances. For low-lying states of each symmetry, the theoretical predictions are in good general agreement with resonances measured in electron-hydrogen atom scattering data.[4] In recent years, as the calculational tools have improved, more attention has been drawn to doubly excited states lying below the higher N ($N \geq 3$) thresholds. Furthermore, recent series of photodetachment studies[5] of H^- in a relativistic H^- beam have improved the energy resolution of these resonances considerably, thus providing a new challenge to the understanding and prediction of these states.

Earlier studies have shown that in resonance states of H^-, there exist certain underlying approximate symmetries. The group theoretical method[6] and the method of solving for two-electron wave functions in hyperspherical coordinates[7-11] have been employed to understand these "hidden" approximate symmetries. While these two methods are probably not sufficiently developed to predict resonance parameters as accurately as other approaches, they do provide information about the nature of the correlated motion of two excited electrons directly. In particular, a recent development in the hyperspherical coordinates approach reveals that the underlying dynamical symmetries are related to the different eigenmodes of the motion of two correlated electrons.[12]

The hyperspherical coordinate method replaces the electron radial coordinates (r_1, r_2) by hyperspherical variables $R=(r_1^2+r_2^2)^{1/2}$ and $\alpha=\arctan(r_2/r_1)$. The variable R measures the "size" of the negative ion. By solving the two-electron Schrödinger equation at fixed values of the coordinate R with R treated as a parameter, the resulting energy eigenvalues $U_\mu(R)$ are then the "potential curves," where μ corresponds to different "channels." Mathematically this is analogous to the Born-Oppenheimer approach in molecular physics. The eigenenergies of doubly excited states of H^- for each channel μ are then the "vibrational energies" calculated from solving a one-dimensional radial equation using the potential curves $U_\mu(R)$. This method of calculating approximate eigenenergies of doubly excited states in hyperspherical coordinates has been applied previously by several workers to two-electron systems,[7-11] to two valence-electron systems,[13,14] and to doubly excited states in three-electron systems.[15,16] The method has also been applied to calculate elastic scattering phase shifts.[17-19] Various numerical techniques have been developed to calculate the potential curves $U_\mu(R)$, but most of these methods are inappropriate for high-lying potential curves. In a recent article,[20] the author reported the newly developed analytical channel functions in hyperspherical coordinates. These new functions simplify the calculation of higher potential curves $U_\mu(R)$. Since the properties of doubly excited states of H^- lying below the $H(N=3)$ thresholds have never been sytematically investigated using that approach, this article de-

scribes its application to these high-lying doubly excited states.

Section II describes the methods used in the calculation of the potential curves. The resulting potential curves $U_\mu(R)$ lying below the H($N=3$) limits are shown in Sec. III for $^{1,3}S^e$, $^{1,3}P^o$, $^{1,3}D^e$, and $^{1,3}P^e$ symmetries, and those lying below the H($N=4$) limits are shown for $^{1,3}S^e$ symmetries. The approximate energy eigenvalues and radial wave functions of autodetaching states are then calculated from the attractive potential curves and are compared with other theoretical calculations in Sec. IV. From the potential curves, it is shown that our classifications of some of these states differ from the recent work of Gailitis.[21] In Sec. V, angular correlations of doubly excited states are investigated.

II. THEORETICAL METHODS

In the adiabatic approximation, the wave function of the nth excited state in channel μ is expressed as

$$\psi^n_\mu(R,\Omega)=R^{-5/2}(\sin\alpha\cos\alpha)^{-1}F^n_\mu(R)\Phi_\mu(R;\Omega)\ , \tag{1}$$

where the adiabatic channel function satisfies the partial differential equation

$$\left[-\frac{1}{R^2}\frac{d^2}{d\alpha^2}+\frac{\vec{l}_1^{\,2}}{R^2\sin^2\alpha}+\frac{\vec{l}_2^{\,2}}{R^2\cos^2\alpha}+\frac{2}{R}\left[-\frac{Z}{\sin\alpha}-\frac{Z}{\cos\alpha}+\frac{1}{(1-\sin 2\alpha\cos\theta_{12})^{1/2}}\right]\right]\Phi_\mu(R;\Omega)$$
$$=U_\mu(R)\Phi_\mu(R;\Phi)\ . \tag{2}$$

In Eqs. (1) and (2), $\Omega\equiv\{\alpha,\hat{r}_1,\hat{r}_2\}$, where $\hat{r}_i=(\theta_i\phi_i)$ denotes the usual spherical angles and $\vec{l}_i$ is the orbital angular momentum operator for electron i, θ_{12} is the angle subtended by the two electrons to the nucleus, and $Z=1$ is the charge of the nucleus. For low-lying doubly excited states, it is convenient to expand $\Phi_\mu(R;\Omega)$ as

$$\Phi_\mu(R;\Omega)=\sum_{l_1l_2q}a^q_{l_1l_2}(R)\phi_{l_1l_2q}(R;\Omega)\ , \tag{3}$$

where the basis function is defined by

$$\phi_{l_1l_2q}(R;\Omega)=\mathscr{A}[g^q_{l_1l_2}(R;\alpha)\mathscr{Y}_{l_1l_2LM}(\hat{r}_1,\hat{r}_2)]\ . \tag{4}$$

In (4), $\mathscr{A}$ is the proper symmetrization or antisymmetrization operator (the spin function is not explicitly considered in this article), $\mathscr{Y}_{l_1l_2LM}(\hat{r}_1,\hat{r}_2)$ is the coupled orbital angular momentum function, and $g_{l_1l_2q}(R;\alpha)$ is the approximate analytical basis function described in Ref. 20. Briefly, within the given $[l_1l_2]$ subspace, these approximate analytical channel functions are obtained as follows: (a) For $l_1=l_2=l$, $g^n_{ll}(R;\alpha)$ is obtained from the r-weighted radial hydrogenic nl wave function $r_1R_{nl}(r_1)$ by replacing r_1 by $R\sin\alpha\cos\alpha$. An additional factor $\cos 2\alpha$ is multiplied by the resulting expression if $L+S=$odd. (b) For $l_1\neq l_2(l_1<l_2)$, the generalized analytical function is obtained (i) by expressing the r-weighted radial hydrogenic nl_1 wave function as

$$r_1R_{nl_1}(r_1)=r_1r_1^{l_1}P_{nl_1}(r_1)e^{-r_1/n}\ ,$$

where $P_{nl_1}(r)$ is the Laguerre polynomial, and (ii) by replacing r_1 by $R\sin\alpha$ and multiplying $(\cos\alpha)^{l_2+1}$ by the resulting expression. For example, (4) is expressed as

$$\phi_{l_1l_2n}=[(\sin\alpha)^{l_1+1}(\cos\alpha)^{l_2+1}P_{nl_1}(R\sin\alpha)e^{-(R\sin\alpha)/n}\mathscr{Y}_{l_1l_2LM}(\hat{r}_1,\hat{r}_2)] \tag{5}$$

for the channel which converges to the hydrogenic nl_1 state in the limit $R\to\infty$. If there are two hydrogenic limits nl_1 and nl_2 for a given n within the $[l_1l_2]$ pair, the other generalized analytical function $\phi_{l_2l_1n}$ is obtained from (5) by interchanging l_1 and l_2. Since nl_1 and nl_2 hydrogenic states are degenerate, the "actual" channel function within $[l_1l_2]$ subspace will be the linear combination of

$\phi_{l_1 l_2 n}$ and $\phi_{l_2 l_1 n}$, resulting in channel functions which have the "+" and "−" characters as originally described by Cooper *et al.*[22] for the doubly excited states of He.

The basis functions (4) are normalized at each R by requiring

$$\int_o^{\pi/2} [g^n_{l_1 l_2}(R;\alpha)]^2 d\alpha = 1 \ . \tag{6}$$

These normalized functions reduce to hydrogenic nl_1 states as $R \to \infty$ and $\alpha \to 0$. In the intermediate-R region, it was shown[20] that the channel functions within the given $[l_1 l_2]$ subspace were well represented by such analytical functions. In the small-R region, such analytical basis functions reduce to hyperspherical harmonics $u_{l_1 l_2 m}$ [which are the exact solutions of (2) at $R=0$] if the channel corresponds to the lowest channel of that particular $[l_1 l_2]$ subspace. For higher channels the analytical channel function does not reduce to hyperspherical harmonics and we remedy the small-R region by including hyperspherical harmonics in the basis set directly. Therefore, in the actual calculation several hyperspherical harmonics and several generalized analytical basis functions (4) are included in the diagonalization of Eq. (2). Since the small-R region is expected to be well represented by hyperspherical harmonics and the large-R region by the generalized analytical channel functions, the basis set required for the diagonalization is small. It is important to point out that previously the potential curves $U_\mu(R)$ were calculated either by solving the coupled differential equations (2) directly or by diagonalization using eigenfunctions $u_{l_1 l_2 m}$ method often suffers from numerical instability when many $[l_1 l_2]$ are included and the second method suffers from slow convergence at large R, where basis $u_{l_1 l_2 m}$ with large values of m are needed in the diagonalization.

III. POTENTIAL CURVES

The potential curves which converge to the $N=3$ threshold and the two lowest curves which lie below the $N=4$ threshold for $^{1,3}S$ symmetries of H^- are shown in Fig. 1. Curves that converge to the $N=3$ threshold for $^{1,3}P^o$, $^{1,3}D^e$ symmetries are shown in Figs. 2(a) to 2(d) and for $^{1,3}P^e$ symmetries are shown in Fig. 3. Lower curves which converge to the $N=1$ and $N=2$ thresholds have been previously calculated[8(a)] using different numerical techniques. The present calculations agree with previous results for these lower channels.

The size of the basis set used in the present calculation is much smaller than those used by Klar and Klar[9] since the basis functions used here are well behaved in both $R \to 0$ and $R \to \infty$ limits. In a typical calculation, for example, to obtain the curves shown in Fig. 1(a), basis functions consisting of hyperspherical harmonics u_{llm} with $(lm)=(02)$, (04), (06), (12), (14), (22), (32), and analytical channel functions ϕ_{lln} with $(ln)=(01)$, (02), (03), (04), (12), (13), (14), (23), (24), (34), and (45) are included in the diagonalization. As illustrated in Ref. 20, because $\phi_{lln}(R;\Omega)$ with $n=l+1$ reduces to $u_{llo}(\Omega)$ as $R \to 0$, the basis functions

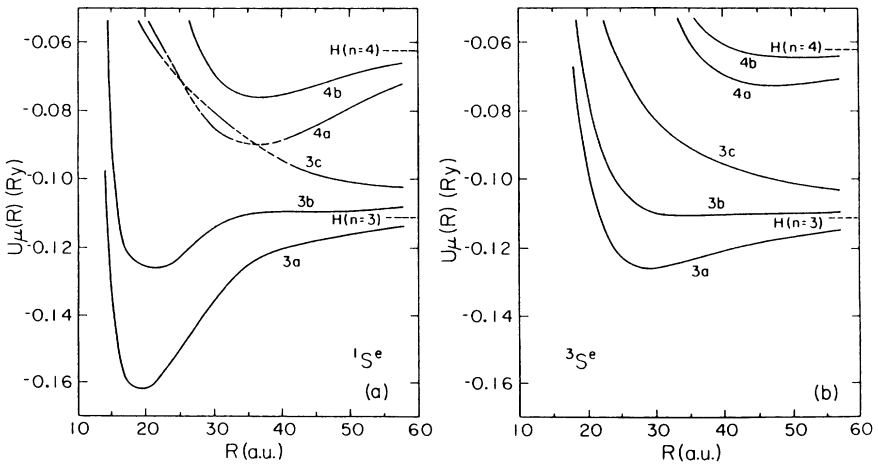

FIG. 1. Potential curves for H^- $^{1,3}S^e$ channels converging to the $N=3$ and $N=4$ limits of H.

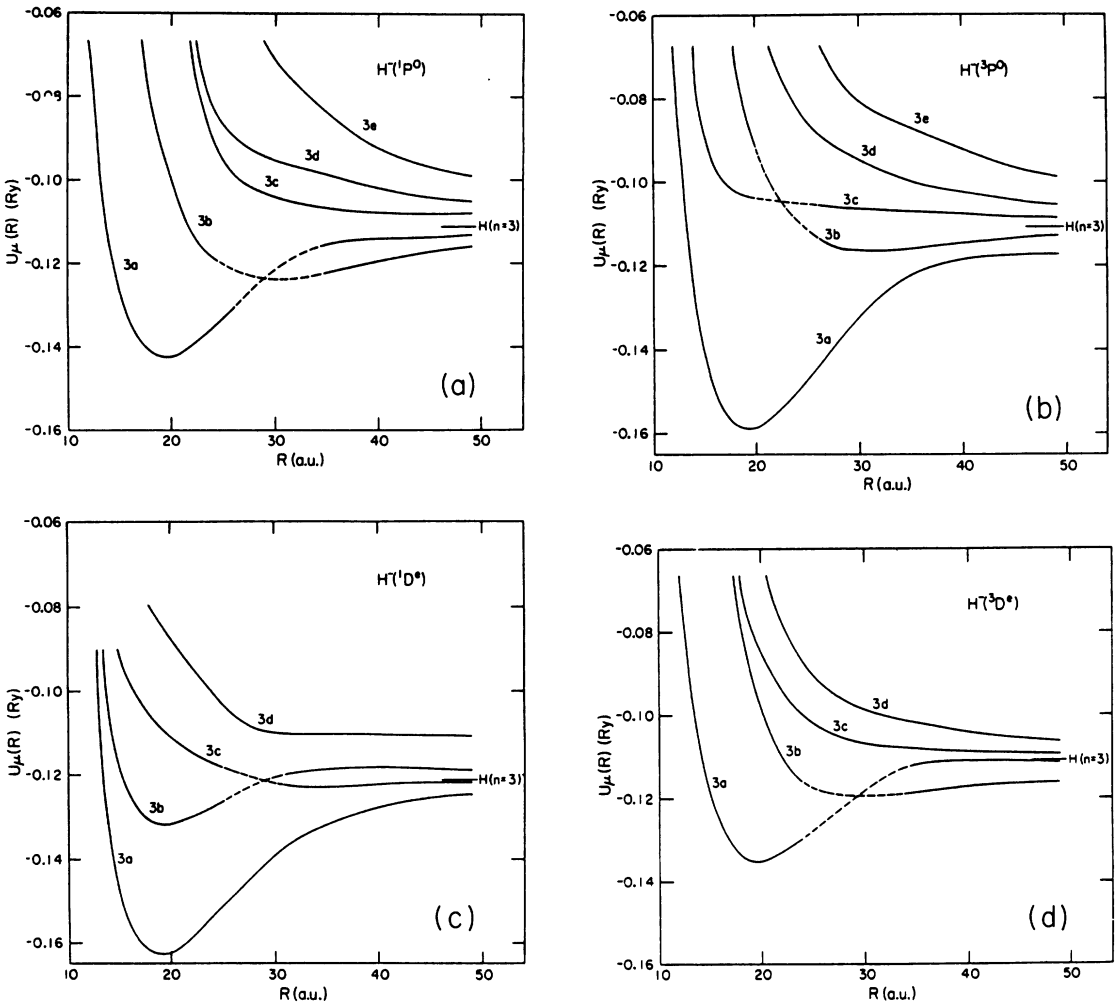

FIG. 2. Potential curves for H^- $^{1,3}P^o$ and $^{1,3}D^e$ channels converging to the $N=3$ limit of H.

$u_{l l_0}(\Omega)$ are not needed in the diagonalization. Since analytical channel functions are *not* orthogonal, any basis function which has a large overlap (>0.9) is automatically rejected in the calculation, so the actual calculation involves a smaller basis set than indicated above.

The potential curves shown in Figs. 1 and 2 are not all adiabatic curves. Indeed, diabatic crossings

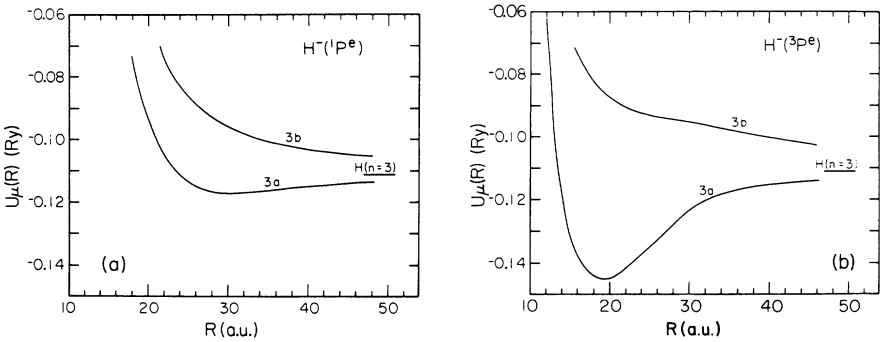

FIG. 3. Potential curves for H^- $^{1,3}P^e$ channels converging to the $N=3$ limit of H.

appear in Fig. 1(a), and in Figs. 2(a)–2(d). These crossings, shown by dashed lines, are drawn by interpolating the calculated adiabatic curves smoothly at points of avoided crossing and allowing the curves to cross. These diabatic curves are preferable to adiabatic ones such that the characters of channel functions $\Phi_\mu(R;\Omega)$ are preserved as R varies. In the case of $L=0$, such characters can be visualized by showing plots of

$$|\Phi_\mu(R;\Omega)|^2 \equiv |\Phi_\mu(R;\alpha,\theta_{12})|^2$$

on the (α,θ_{12}) plane.[12] For example, such plots (Fig. 4, Ref. 12) revealed that charge-density concentrates near the Wannier point ($\alpha=45°$, $\theta_{12}=180°$) for channel $4a$ but concentrates mostly in the smaller θ_{12} region for channel $3c$. In fact, channels $4a$ and $3c$ cross twice in Fig. 1(a). Such crossing can also be detected by observing the variation of the dominant expansion coefficients $a_{l_1 l_2 q}$ with R, by the large values of $\langle \Phi_\mu | d\Phi_\nu/dR \rangle$ near the crossing point or by the degree of angular correlations, as measured by the average value of θ_{12} (see Sec. V). Single crossings are observed between channels $3a$ and $3b$ for $^1P^o$ and $^3D^e$ and between channels $3b$ and $3c$ for $^3P^o$ and $^1D^e$. Such crossings originate from the fact that exchange plays a more important role in determining the energy eigenvalue $U_\mu(R)$ at small R, while at large R, it is dominated by the linear Stark effect of dipole coupling (see Sec. IV). A similar crossing has been observed between the + and − channels (corresponding to channels $2a$ and $2b$ in the present notation, respectively) in $^1P^o$ below the $N=2$ threshold.[8(c)]

IV. CLASSIFICATION OF RESONANCES AND RADIAL WAVE FUNCTIONS

The eigenvalues and radial wave functions for each asymptotically attractive potential $U_\mu(R)$ are obtained by solving the equation

$$\left[\frac{d^2}{dR^2} - U_\mu(R) + 2E_\mu^n\right] F_\mu^n(R) = 0$$

for the nth excited state of channel μ. As described by Seaton[23] and by Gailitis and Damburg,[24] because of the degeneracy of hydrogenic $3s$, $3p$, and $3d$ states (except for the fine-structure splitting $\Delta\epsilon \sim 0.2\ \mathrm{cm}^{-1}$) which are coupled to form a permanent dipole moment, the asymptotic form of the potential curves converging to the $N=3$ threshold behaves as

$$U_\mu(R) \underset{R\to\infty}{\to} -\tfrac{1}{9} + a_\mu/R^2 \ \text{(in Ry)} . \tag{8}$$

It is known that if a_μ is negative and $|a_\mu| > \frac{1}{4}$, then the asymptotic dipole potential itself is strong enough to support an infinite number of bound states. For such a dipole potential, the energy eigenvalues obey the exponential law

$$\frac{E_\mu^n}{E_\mu^{n+1}} \equiv R_\mu = e^{2\pi/\lambda_\mu} , \tag{9}$$

where $\lambda_\mu = |a_\mu + \frac{1}{4}|^{1/2}$, and E_μ^n is evaluated from the H($N=3$) threshold. The potential curves shown in Figs. (1)–(3) follow Eq. (8) only in the large-R region; the more attractive wells at smaller R are attributed to the strong correlations. On the other hand, for the high-lying states of each channel, the states are supported primarily by the asymptotic dipole potential and Eq. (9) is then approximately satisfied. Recently, Gailitis[21] used Eq. (9) to classify the resonances below the $N=3$ thresholds calculated by other workers. Since Eq. (9) is not valid for the lower members of each series and the channels are *not* determined *solely* by the asymptotic dipole potentials, some of his classification turns out to be erroneous.

In Table I the energies from threshold for the resonances in meV are given in accordance with the channels labeled in Figs. 1, 2, and 3 and in terms of Herrick's[6] quantum numbers K and T. In converting Rydbergs into electron volts, 1 Ry = 13.598 42 eV was used to account for finite nuclear mass effects. For each channel μ, the parameters a_μ and R_μ are also given. The calculated eigenvalues E_μ^n from the potential curves are compared with recent calculations of Lipsky *et al.*[25] and of Morgen *et al.*[26] Earlier calculations are not included in the tabulation here.[27] With the aid of potential curves presented in Sec. III, we believe that resonances below the $N=3$ threshold calculated by Lipsky *et al.* and by Morgen *et al.* are correctly classified in Table I. Our channel assignment differs from Gailitis's classification for $^3P^o$ and $^1D^e$ states.

The misclassification of Gailitis originates from the fact that curves $3a$ and $3b$ cross for $^1P^o$ and $^3D^e$ but not for $^3P^o$ and $^1D^e$. The parameters a_μ and R_μ reflect the asymptotic dipole coupling but *without* providing information about the strength of electron correlations at small R. The more attractive $^1P^o$ potential curve is the $3a$ channel, corresponding to $(K,T)=(1,1)$ in Herrick's notation, with asymptotic dipole coefficient $a_\mu = -5.16$; the more attractive $^3P^o$ potential curve

TABLE I. Channel classifications for doubly excited states of H^- lying below the $N=3$ and $N=4$ hydrogenic thresholds. The calculated energies are from the present hyperspherical coordinate approach, from the results of Lipsky *et al.* (Ref. 25) and from Morgen *et al.* (Ref. 26) with the present classification scheme. For $^3P^o$ and $^1D^e$ states, this classification differs from the one presented by Gailitis (Ref. 21). The energies are given in meV's from the thresholds where the conversion 1 Ry = 13.598 42 eV has been used. Channels are designated using the symbols in Figs. 1–3, as well as the quantum numbers (K,T) used by Herrick. Asymptotic dipole potential parameters a_μ [cf. Eq. (8)] and energy ratios R_μ [cf. Eq. (9)] for each channel are also given.

$^1S^e$	Channel $3a$	$(K,T)=(2,0)$	$a_\mu=-16.199$	$R_\mu=4.82$
	$(3a,1)^a$	347.7[b]	369.7[c]	364.4[d]
	$(3a,2)$	52.8	61.5	58.2
	$(3a,3)$	10.8	11.8	
$^3S^e$	Channel $3a$	$(K,T)=(2,0)$	$a_\mu=-16.199$	$R_\mu=4.82$
	$(3a,1)^a$	90.8[b]	93.1[c]	92.1[d]
	$(3a,2)$	18.2	18.5	13.8
	$(3a,3)$	3.7	1.3	
$^1P^o$	Channel $3a$	$(K,T)=(1,1)$	$a_\mu=-5.220$	$R_\mu=16.75$
	$(3a,1)^a$	151.0[b]	184.5[c]	190.9[d]
	$(3a,2)$	4.9	8.8	6.7
	Channel $3b$	$(K,T)=(2,0)$	$a_\mu=-14.897$	$R_\mu=5.16$
	$(3a,1)^a$	72.1[b]	82.0[c]	80.5[d]
	$(3a,2)$	13.6	14.9	10.1
$^3P^o$	Channel $3a$	$(K,T)=(2,0)$	$a_\mu=-14.897$	$R_\mu=5.16$
	$(3a,1)^a$	335.4[b]	342.2[c]	334.6[d]
	$(3a,2)$	48.4	52.2	49.4
	$(3a,3)$	9.3	9.7	
	Channel $3b$	$(K,T)=(1,1)$	$a_\mu-5.220$	$R_\mu=16.75$
	$(3b,1)^a$	17.7[b]	22.3[c]	
$^1D^e$	Channel $3a$	$(K,T)=(2,0)$	$a_\mu=-12.249$	$R_\mu=6.13$
	$(3a,1)^a$	267.8[b]	279.5[c]	281.5[d]
	$(3a,2)$	32.1	34.4	32.9
	$(3a,3)$	5.2	4.8	
	Channel $3b$	$(K,T)=(1,1)$	$a_\mu=-2.30$	$R_\mu=80.55$
	$(3b,1)^a$	6.3[b]	4.9[c]	
$^3D^e$	Channel $3a$	$(K,T)=(1,1)$	$a_\mu=-2.30$	$R_\mu=80.55$
	$(3a,1)^a$	78.9[b]	104.3[c]	92.0[d]
	$(3a,2)$	0.5	0.26	
	Channel $3b$	$(K,T)=(2,0)$	$a_\mu=-12.249$	$R_\mu=6.13$
	$(3b,1)^a$	67.2[b]	59.4[d]	57.9[d]
	$(3b,2)$	10.5	9.1	4.2
$^1P^e$	Channel $3a$	$(K,T)=(1,1)$	$a_\mu=-5.219$	$R_\mu=16.75$
	$(3a,1)^a$	16.0[b]	22.8[c]	

TABLE I. (*Continued.*)

$^3P^e$	Channel $3a$	$(K,T=(1,1)$	$a_\mu=-5.219$	$R_\mu=16.75$
	$(3a,1)$[a]	179.5[b]	191.4[c]	
	$(3a,2)$	6.0	9.4	
$^1S^e$	Channel $4a$	$(K,T)=(3,0)$	$a_\mu=-33.321$	$R_\mu=2.98$
	$(4a,1)$[a]	244.8[b]	234.9[e]	227.7[f]
	$(4a,2)$	70.4	77.7	94.2
$^3S^e$	Channel $4a$	$(K,T)=(3,0)$	$a_\mu=-33.321$	$R_\mu=2.98$
	$(4a,1)$[a]	82.1[b]	85.5[e]	
	$(4a,2)$	27.8	27.5	

[a] (μ,n) nth state of channel μ.
[b] Present calculations.
[c] Lipsky *et al.* (Ref. 25).
[d] Morgen *et al.* (Ref. 26).
[e] Oberoi [Ref. 27(d)].
[f] Ho (Ref. 29).

belongs to the $3a$ channel but has corresponding $(K,T)=(2,0)$, and $a_\mu=-16.75$. A similar switchover also occurs for $^1D^e$ and $^3D^e$.

The lowest eigenvalues for each L and S given in Table I, as calculated in the present approach, are probably not as accurate as those obtained by other methods. A more accurate result may be obtained by including off-diagonal coupling terms. On the other hand, higher members of each series and even the lowest member of the less attractive channels are probably more accurately calculated in the present work. These high-lying states are very diffuse and are supported primarily by the dipole potentials. Other variational approaches are designed usually for the more tight-binding states and often do not describe these diffuse orbitals adequately. In Fig. 4(a) the radial wave functions $F^1_\mu(R)$ for the lowest member of channels $\mu=3a$ and $4a$ for $^{1,3}S^e$ states are shown. These graphs illustrate the "size" of the states. Similar graphs for the two lowest members of channels $3a$ and $3b$ for $^1P^o$ states are shown in Fig. 4(b) and the three lowest members of the $\mu=3a\,^3P^o$ states are shown in Fig. 4(c). Notice the diffuseness of the high-lying states shown in Figs. 4(b) and 4(c).

The potential curves shown in Fig. 2(a) for $^1P^o$ states have previously been calculated by Greene[11] in connection with the interpretation of Feshbach resonances below the $N=3$ threshold in H^- photodetachment measurement by Hamm *et al.*[28] Greene's calculations differ from the present one in that basis with $(l_1l_2)=(2,3)$ are not included and Eq. (2) is solved numerically. In addition, the second-order diagonal coupling term $(\Phi_\mu\,|\,d^2\Phi_\mu/dR^2)$ is included in $U_\mu(R)$ in the present work but not in Greene's. Notice that channel $3a$ corresponds to the usual $+$ channel and channel $3b$ to the usual $-$ channel. The $+$ channel (or $3a$ channel) is more easily populated in a collision and, in fact, both of the two resonances observed in the experiment of Hamm *et al.* belong to the $\mu=3a$ channel.

V. ANGULAR CORRELATIONS

Doubly excited states often exhibit strong radial and angular correlations not familiar in singly excited states. While radial correlations—as measured by the distribution of charge density in angle α—diminish at large R, angular correlations persist even at large R. For $L=0$ states, this high degree of angular correlation can be visualized directly by displaying the surface charge-density plots $|\phi_\mu(R;\Omega)|^2$ on the (α,θ_{12}) plane. It was shown in Ref. 12 that the distribution of $|\Phi_\mu(R;\Omega)|^2$ for each channel μ remains relatively constant as R increases. For $L\neq0$ states it is more difficult to visualize $|\Phi_\mu(R;\Omega)|^2$ directly since the internal coordinates α and θ_{12} cannot be conveniently separated from the angles which describe the overall rotation of the system. In this section, it will be shown that doubly excited states with $L\neq0$ also exhibit strong angular correlations similar to $L=0$ states.

To show the degree of angular correlations, we define the average angle $\langle\theta_{12}\rangle$ by

$$\cos\langle\theta_{12}\rangle_\mu=\langle\Phi_\mu(R;\Omega)\,|\,\cos\theta_{12}\,|\,\Phi_\mu(R;\Omega)\rangle\ , \tag{10}$$

where the integration is over all the angles Ω.

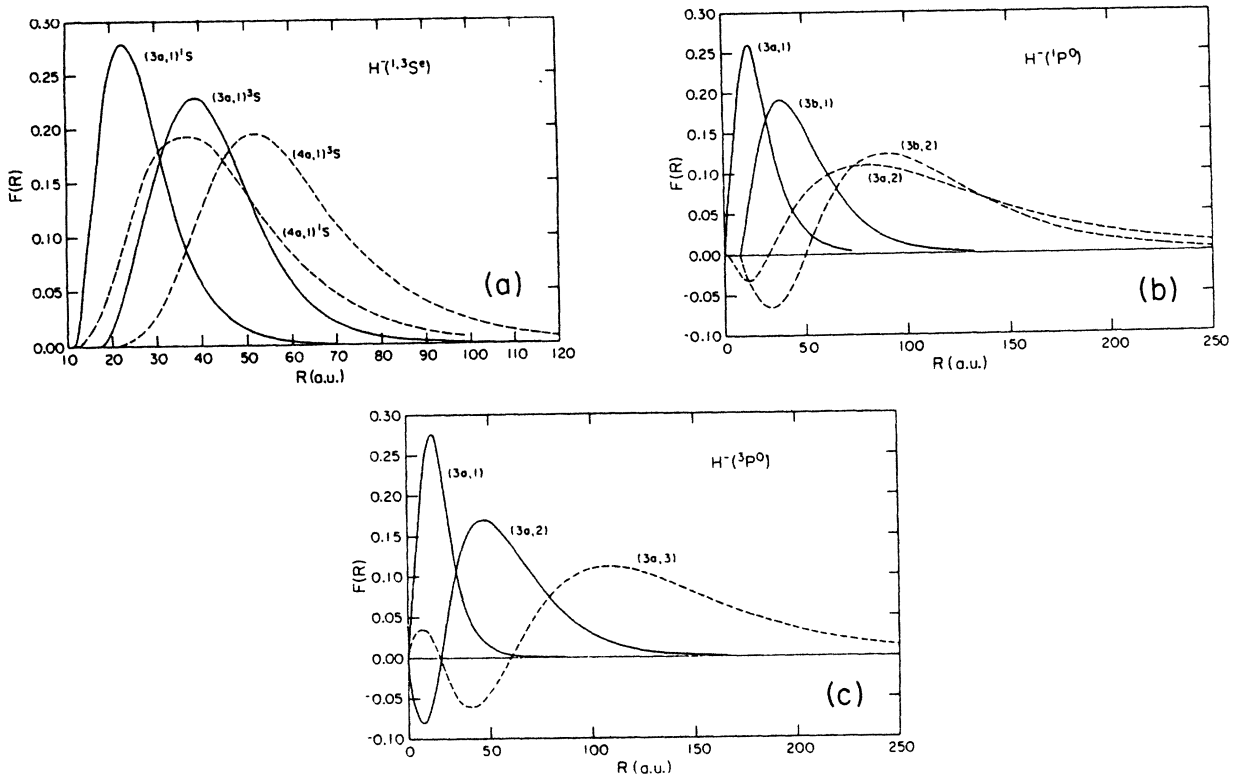

FIG. 4. Radial wave functions of some doubly excited states of H^-; (a) for the lowest state for $^{1,3}S^e$ lying below $H(N=3)$ and $H(N=4)$ thresholds, (b) for the two lowest states of channel $3a$ and channel $3b$ of $^1P^o$; (c) for the three lowest states of channel $3a$ of $^3P^o$.

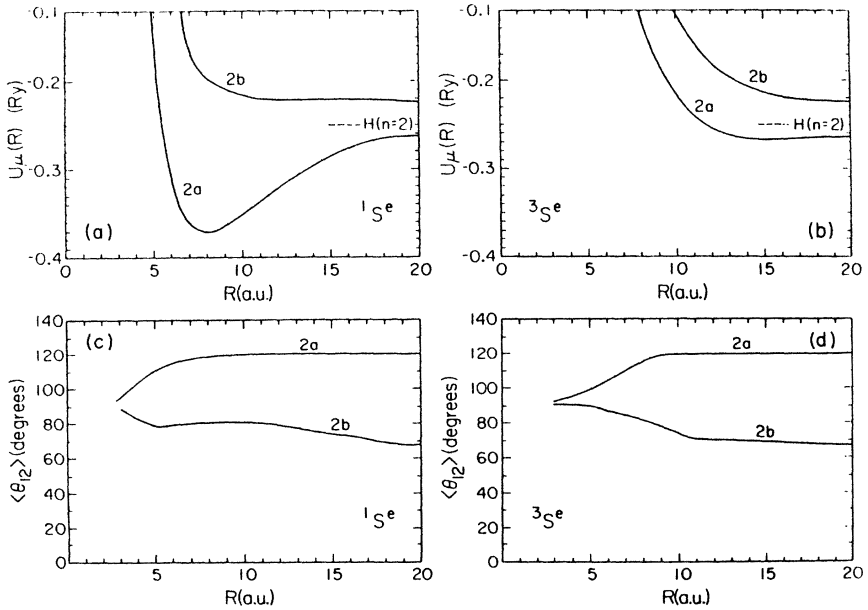

FIG. 5. Potential curves for H^- $^{1,3}S^e$ channels and the average angle $\langle\theta_{12}\rangle$ for the two channels converging to the $N=2$ threshold of H.

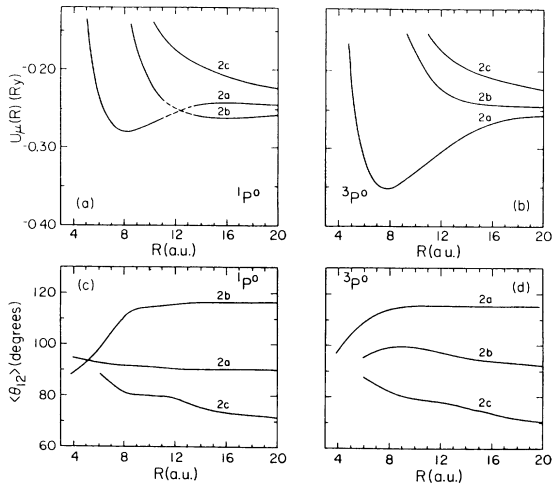

FIG. 6. Same as Fig. 5 except for $^{1,3}P^o$ channels.

This definition is simple, but is not the most suitable one since states which are not correlated correspond to $\langle\theta_{12}\rangle=90°$. On the other hand, this is not serious since doubly excited states always exhibit strong angular correlations [through the strong mixing of different (l_1,l_2) pairs in Eq. (3)] and since the angle $\langle\theta_{12}\rangle_\mu$ provides a qualitative description of angular correlations between the two electrons for each channel μ.

In Fig. 5 the variations of $\langle\theta_{12}\rangle_\mu$ with R for the two lowest doubly excited channels for $^1S^e$ and $^3S^e$ states of H^- are shown. For comparison the relevant potential curves are also shown. Two important aspects are easily observed: (1) $\langle\theta_{12}\rangle_\mu$ is independent of R for the intermediate- and the large-R regions; (2) $\langle\theta_{12}\rangle_\mu$ differs greatly for

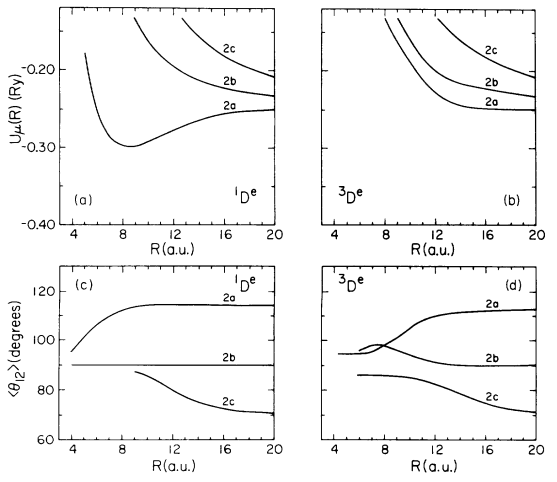

FIG. 7. Same as Fig. 5 except for $^{1,3}D^e$ channels.

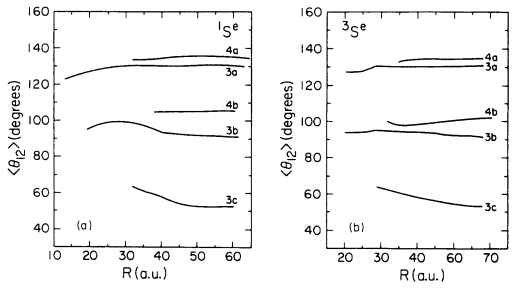

FIG. 8. Average angle $\langle\theta_{12}\rangle$ for H^- $^{1,3}S^e$ channels converging to the $N=3$ and $N=4$ thresholds of H. Refer to Fig. 1 for the potential curves.

$\mu=2a$ and $2b$. [For our purpose of discussion, the small-R region for each channel μ is defined for values of R, where the potential curve $U_\mu(R)$ is highly repulsive. The intermediate-R region is defined for attractive curves as where the potential wells lie and for repulsive curves as where the potential curves begin to flatten out.] In Fig. 5 we notice that $\langle\theta_{12}\rangle\sim120°$ for $\mu=2a$ and $\sim60°$ for $\mu=2b$, thus the two electrons tend to stay on opposite sides of the nucleus for $\mu=2a$ and to stay on the same side of the nucleus for $\mu=2b$. These results are independent of whether $S=0$ or $S=1$.

In Fig. 5 the average $\langle\theta_{12}\rangle$ varies quite rapidly in the small-R region. Since the channel function $\Phi_\mu(R;\Omega)$ is obtained by an adiabatic approximation, this rapid variation clearly suggests that adiabatic channel functions may not be appropriate for higher excited states of each channel. In fact, existing calculations for the high-lying states and scattering phase shifts indicated that the adiabatic approximation is not very suitable.[17–19]

It must be emphasized that one should not view $\langle\theta_{12}\rangle$ as the "angle" between the two electrons. As shown in Ref. 12, the actual surface charge density $|\Phi_\mu(R;\alpha,\theta_{12})|^2$ is peaked at $\theta_{12}=\pi$ for $\mu=2a$ and concentrated mostly in the region $\theta_{12}>\pi/2$. For $\mu=2b$, the surface charge density shows concentration in the region $\theta_{12}\leq\pi/2$ with a peak near $\theta_{12}=0$ (see Fig. 5, Ref. 12). In Figs. 6 and 7, $\langle\theta_{12}\rangle_\mu$ and $U_\mu(R)$ for $\mu=2a$, $2b$, and $2c$ are shown, respectively, for $^{1,3}P^o$ and $^{1,3}D^e$ states. The angle $\langle\theta_{12}\rangle_\mu$ for each channel remains roughly constant in the intermediate- and large-R regions and they differ quite substantially between the channels, indicating different angular correlations in these channels. In comparison with Fig. 5, we notice that the largest $\langle\theta_{12}\rangle$ reduces from 120° for $^{1,3}S^e$ to 116° for $^{1,3}P^o$ and to 114° for $^{1,3}D^e$ and the smallest $\langle\theta_{12}\rangle$ increases from 60° for $^{1,3}S^e$ to approximately 70° for $^{1,3}P^o$ and $^{1,3}D^e$ and the channel

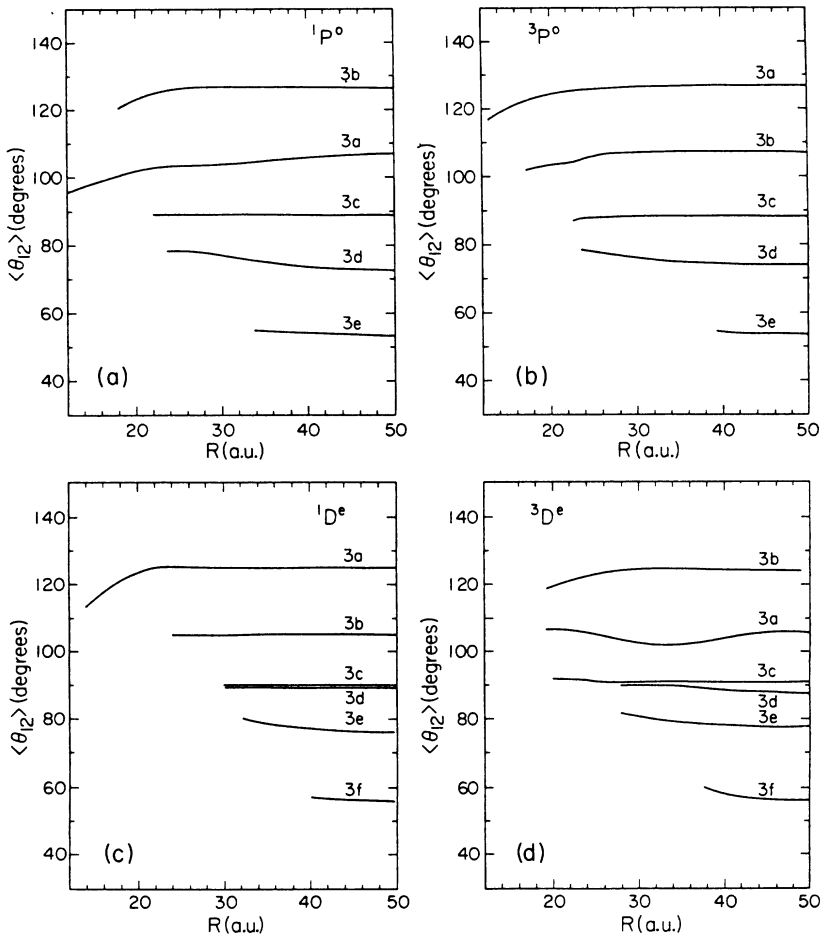

FIG. 9. Average angle $\langle\theta_{12}\rangle$ for H^- $^{1,3}P^o$ and $^{1,3}D^e$ channels converging to the $N=3$ thresholds of H. Refer to Fig. 2 for the potential curves.

in the middle has $\langle\theta_{12}\rangle=90°$. Thus the overall orbital angular momentum of the system has only minor effect on angular correlations. Notice that $\langle\theta_{12}\rangle_\mu$ for each channel is *not* constant in the small-R region and the results are independent of whether $S=0$ or $S=1$.

We once again point out the crossing of the two curves $2a$ and $2b$ for $^1P^o$. This crossing is *necessary* if $\langle\theta_{12}\rangle$ is to remain constant with respect to R for each channel. In general, one would expect that large $\langle\theta_{12}\rangle$ corresponds to lower $U_\mu(R)$ because of smaller Coulomb repulsion due to the two electrons. This would be the case if angular correlation were the sole factor in determining the potentail energy $U_\mu(R)$. In fact, we see this is *not* the case for $^1P^o$. The $-$ channel ($2b$ in Fig. 5), which has largest $\langle\theta_{12}\rangle$, although having lowest potentials at large R, is actually more repulsive at smaller R than the $+$ channel ($2a$ in Fig. 5). At larger R, there is no radial correlation and the $-$ channel which has $\langle\theta_{12}\rangle\sim116°$ has lower potential than the $+$ channel which has $\langle\theta_{12}\rangle\sim90°$. At smaller R where radial correlations are important, the $+$ channel achieves lower potentials by exhibiting a higher degree of radial correlation and the channel function shows large amplitude near $\alpha=\pi/4(r_1\sim r_2)$. On the other hand, the $-$ channel, with a node near $\alpha=\pi/4$, has higher potentials.[8(a)]

The angular correlations for the channels that converge to the higher hydrogenic thresholds are shown in Figs. 8 and 9. The relevant potential curves are shown in Figs. 1 and 2 where the intermediate- and large-R regions can be specified. We again notice that $\langle\theta_{12}\rangle_\mu$ for each channel remains almost constant after passing the small-R region. The diabatic crossings in $U_\mu(R)$ in Figs. 1 and 2 are made necessary if $\langle\theta_{12}\rangle_\mu$ for each chan-

nel in the intermediate- and large-R regions is to stay constant.

VI. SUMMARY

In this article the properties of doubly excited states lying below $H(N=3)$ and $H(N=4)$ thresholds are investigated in hyperspherical coordinates. With the recently developed analytical channel functions, it is feasible to calculate the large number of adiabatic potential curves corresponding to high-lying doubly excited states. It is found that diabatic crossing between the curves is often needed if the channels are to maintain their characters. The role of radial and angular correlations are also discussed. While the dipole coupling, as a result of angular correlation and of the degeneracy of hydrogenic excited states, is the only important factor in determining the potential energy curves at large hyper-radii R, radial correlations, which are not incorporated in the dipole coupling, are important at small R. These two competitive correlations are both important in deciding the properties of doubly excited states. Classifications of doubly excited states based upon angular correlations alone will end up with erroneous results. Angular correlations for doubly excited states below $H(N=2)$ and $H(N=3)$ thresholds are also investigated. It is found that each channel possesses constant angular correlations in the intermediate- and large-R regions but not in the repulsive small-R region. It appears that breakdown of the adiabatic approximation occurs predominately in the small-R region but this subject will be delayed for future study.

This work was supported in part by the U. S. Department of Energy, Division of Chemical Sciences, and in part by the Alfred P. Sloan Foundation.

[1]A. J. Taylor and P. G. Burke, Proc. Phys. Soc. London 92, 336 (1967); P. G. Burke, A. J. Taylor, and S. Ormonde, *ibid.* 92, 345 (1967).

[2]K. T. Chung and J. C. Y. Chen, Phys. Rev. A 6, 686 (1972); A. K. Bhatia and A. Temkin, *ibid.* 8, 2184 (1973); G. W. F. Drake and A. Dalgarno, Proc. R. Soc. London, Sect. A 320, 549 (1971).

[3]J. T. Broad and W. P. Reinhardt, Phys. Rev. A 14, 2159 (1976).

[4]See G. J. Schulz, Rev. Mod. Phys. 49, 378 (1973); J. S. Risley, in *Atomic Physics 4,* edited by G. Zu. Putlitz, E. B. Weber, and A. Winnacker (Plenum, New York, 1975).

[5]See the review by H. C. Bryant *et al.*, in *Atomic Physics 7,* edited by D. Kleppner and F. M. Pipkin (Plenum, New York, 1981).

[6]D. R. Herrick and O. Sinanoglu, Phys. Rev. A 11, 97 (1975).

[7]J. H. Macek, J. Phys. B 1, 831 (1968).

[8](a) C. D. Lin, Phys. Rev. A 10, 1986 (1974); (b) *ibid.* 12, 493 (1975); (c) Phys. Rev. Lett. 35, 1150 (1975).

[9]H. Klar and M. Klar, J. Phys. B 13, 1057 (1980).

[10]U. Fano, in *Atomic Physics I,* edited by B. Bederson, V. W. Cohen, and F. M. Pichanick (Plenum, New York, 1969), p. 209; see also U. Fano, Phys. Today 29, No. 9, 32 (1976).

[11]C. H. Greene, J. Phys. B 13, L39 (1980).

[12]C. D. Lin, Phys. Rev. A 25, 76 (1982).

[13]C. H. Greene, Phys. Rev. A 23, 661 (1981).

[14]C. D. Lin (unpublished).

[15]C. W. Clark and C. H. Greene, Phys. Rev. A 21, 1786 (1980).

[16]S. Watanabe, Phys. Rev. A (in press).

[17]C. D. Lin, Phys. Rev. A 12, 493 (1975).

[18]H. Klar and M. Klar, Phys. Rev. A 17, 1007 (1978).

[19]D. Miller and A. F. Starace, J. Phys. B 13, L525 (1980).

[20]C. D. Lin, Phys. Rev. A 23, 1585 (1981).

[21]M. Gailitis, J. Phys. B 13, L479 (1980).

[22]J. W. Cooper, U. Fano, and F. Prats, Phys. Rev. Lett. 10, 518 (1963).

[23]M. J. Seaton, Proc Phys. Soc. London 77, 174 (1961).

[24]M. Gailitis and R. Damburg, Proc Phys. Soc. London 82, 192 (1963).

[25]L. Lipsky, R. Anania, and M. J. Conneely, At. Data Nucl. Data Tables 20, 127 (1977).

[26]L. A. Morgen, M. R. C. McDowell, and J. Callaway, J. Phys. B 10, 3297 (1977).

[27]More complete tabulation can be found in Ref. 21. Such calculations can be found in (a) P. G. Burke, S. Ormonde, and W. Wittaker, Proc. Phys. Soc. London 92, 319 (1967); (b) K. T. Chung, Phys. Rev. A 6, 1809 (1972); (c) Y. K. Ho, J. Phys. B 10, L373 (1977); (d) R. S. Oberoi, J. Phys. B 5, 1120 (1972).

[28]M. E. Hamm, R. W. Hamm, J. Donahue, P. A. M. Gram, J. C. Pratt, M. A. Yates, R. D. Bolton, P. A. Clark, H. C. Bryant, C. A. Frost, and W. W. Smith, Phys. Rev. Lett. 43, 1715 (1979).

[29]Y. K. Ho, J. Phys. B 12, L543 (1979).